# Low detection limit sensor based on subwavelength grating racetrack resonator

Lijun Huang[a,b,*], Hai Yan[a], Xiaochuan Xu[c,*], Swapnajit Chakravarty[c], Naimei Tang[c], Huiping Tian[b,*], Ray T. Chen[a,c,*]

[a]Dept. of Electrical and Computer Engineering, The University of Texas at Austin, Austin, TX, USA 78758;

[b]State Key Laboratory of Information Photonics and Optical Communications, School of Information and Communication Engineering, Beijing University of Posts and Telecommunications, Beijing, China 100876;

[c]Omega Optics Inc., 8500 Shoal Creek Blvd., Austin, TX, USA 78759

## ABSTRACT

Subwavelength grating (SWG) ring resonators have demonstrated better sensitivity compared to the conventional silicon strip ring resonators due to the enhanced photon-analyte interaction. As the sensors are usually used in absorptive ambient environment, it is extreme challenging to further improve the sensitivity of the SWG ring resonator without deteriorating the quality factor because the coupling strength between the bus waveguide and the circular ring resonator is not sufficient to compensate the loss. To explore the full potential of the SWG ring resonator, we experimentally demonstrate a silicon-based high quality factor and low detection limit transverse magnetic (TM) mode SWG racetrack resonator around 1550 nm. A quality factor of 9800 is achieved in aqueous environment when the coupling length and gap are equal to 6.5 μm and 140 nm, respectively. The bulk sensitivity (S) is ~429.7 nm/RIU (refractive index per unit), and the intrinsic detection limit (*i*DL) is $3.71\times10^{-4}$ RIU reduced by 32.5% compared to the best value reported for SWG microring sensors.

**Keywords:** Subwavelength structures; Gratings; Optical sensing and sensors; Integrated optics devices.

* hljnet@163.com, xiaochuan.xu@omegaoptics.com, hptian@bupt.edu.cn, chenrt@austin.utexas.edu

## INTRODUCTION

Silicon-on-insulator (SOI) platform based sensors has been intensively investigated for point-of-care applications. Various resonance structures have been proposed to optimize the performance of these sensors, such as two-dimensional photonic crystal (PhC) micro-cavity resonators [1-4], one dimensional PhC nanobeam resonators [5-8], disk resonators [9, 10], and ring resonators [11-13]. Ideally, these sensors require a high quality factor, high sensitivity and low limit of detection, which strongly are limited to the optical loss, the overlap of light and analytes, the light polarization. Several different recipes have been demonstrated to enhance the photon-analyte interaction and sensitivity by confining light in the low refractive index region. These sensors include ring slot resonators [14, 15], slot waveguides [16], nano-holes [17], low index modes [8], and transverse magnetic (TM) guide modes [9, 10].

Recently, silicon photonic micro-ring resonator based on photon-analyte interaction has been reported, which can match and even exceed the detection limit of ELISA (subpicogram/mL) by applying the nanoparticle-clustering methodology to the micro-ring resonator assay [18]. Thus, the photon-analyte interaction is more intense when the evanescent field penetrates deeper into the cladding. Subwavelength grating (SWG) waveguide that consists of periodic silicon pillars can increase the light and the cladding materials interaction on the top and side of the waveguide, and the space between the silicon pillars on the light propagation path [13]. Intuitively, compared to a standard silicon strip waveguide resonator with the same cross-section, silicon photonic micro-ring resonator based on SWG waveguide can enhance the photon-analyte interaction. Therefore, a higher sensitivity can be expected. However, the increased interaction inevitably causes additional absorption loss by analytes and scattering loss induced by surface roughness in the micro-ring region, thus, the quality factor ($Q$) of micro-ring resonator would then deteriorate. As a result, for certain wavelength $\lambda$, the intrinsic

Nanoscale Imaging, Sensing, and Actuation for Biomedical Applications XIV, edited by Alexander N. Cartwright, Dan V. Nicolau, Dror Fixler, Proc. of SPIE Vol. 10077, 100770M © 2017 SPIE · CCC code: 1605-7422/17/$18 · doi: 10.1117/12.2252429

detection limit ($i$DL = $\lambda/S{\cdot}Q$) that reflects the detection capability of the change of solution concentration may not be enhanced.

In this paper, in order to increase the photon-analyte interaction to increase the sensitivity without decrease the qualify factor, and minimize the detection of limit, a silicon-based high quality factor and low detection limit transverse magnetic (TM) mode SWG racetrack resonator (SWGRTR) around 1550 nm is experimentally demonstrated. The composite subwavelength waveguide core and racetrack ring are formed by periodically interleaving high and low refractive index materials. The experimental results show that a quality factor of 9800 is achieved in water environment when the coupling length and gap are equal to 6.5 μm and 140 nm, respectively. The bulk sensitivity (S) is ~429.7 nm/RIU (refractive index per unit), and the enhanced intrinsic detection limit ($i$DL) of $3.71\times10^{-4}$ RIU are achieved, which marks a reduction of 32.5% compared to the best value reported for SWG microring sensors.

## DEVICE SIMULATION AND ANALYSIS

Fig. 1(a) shows the schematic of the proposed SWGRTR. The magnified image between bus SWG waveguide and the SWG racetrack waveguide is shown in Fig. 1(b). The composite subwavelength waveguide core is formed by periodically interleaving high (silicon) and low (analyte solutions) refractive index materials [19, 20]. To get lower eigen-frequency and increase the photo-analyte overlap, a period of 200nm is chosen. In Fig. 1(b), $\Lambda$ represents the period of the SWG structure and equals 200 nm. $L$, $W$ and $H$ are the length, width and thickness of silicon (Si) pillars, respectively. $L_c$ and $G$ represent the coupling length and the gap between the SWG waveguide and racetrack waveguide, respectively. The radius of racetrack is 10μm. The thickness of the buried oxide is 3μm. The upper cladding is the analyte solutions to be detected.

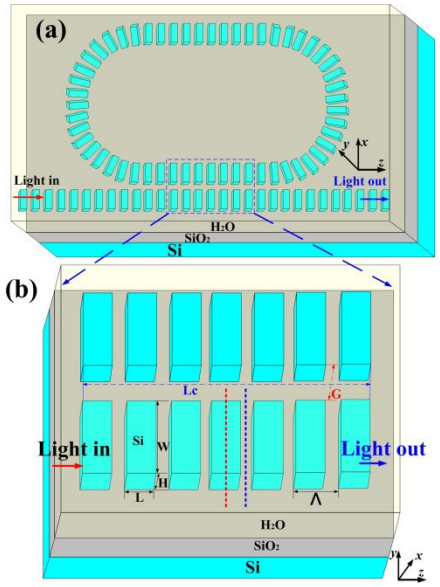


Fig. 1. (a) The 3D schematic of the proposed SWGRTR. (b) The magnified image of the SWG bus waveguide and the SWG racetrack waveguide in rectangular region with a blue dash line.

To analyze the electric field outside Si pillars around 1550 nm, TM mode profiles (RSoft 3D BandSOLVE simulations) on $xy$ plane at different cutting positions (red and blue dash line in Fig. 1(b)) are shown in Fig. 2. The dimension of the silicon pillar ($L\times W\times H$) in this simulation is 140 nm×600nm ×220nm. As seen in Fig. 2, the $y$ component of the electric field extends into the upper cladding and lower substrate. That means the evanescent field penetrates deeply in the cladding and substrate. The more presence of electrical field in analytes is expected to drastically increase the photon-analyte interaction and subsequently enhance both the bulk and surface sensitivity compared with transverse electric (TE) guide modes. However, the increased interaction inevitably causes additional absorption loss by analytes and scattering loss induced by surface roughness. Therefore, a tradeoff between the photon-analyte interaction and optical loss need to be considered in optimizing the design.

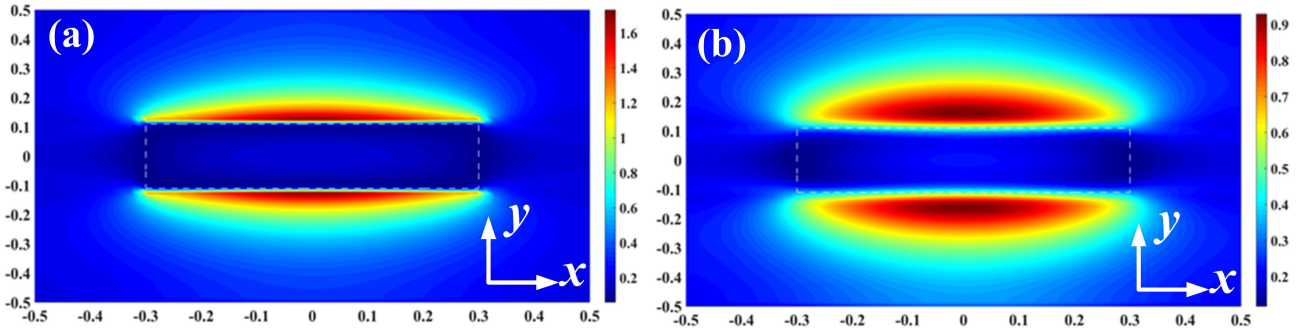


Fig. 2. The $E_y$ electric fields of the TM mode within the silicon pillar to enhance the photon-analyte interaction with $L\times W\times H$ of 140 nm×600nm ×220nm in $xy$ plane in red (a) and blue (b) dash line position in Fig. 1 (b) around 1550 nm.

In order to quantify the photon-analyte interaction and the potential of the proposed SWGRTR structure for sensing applications, we calculate the overlap integral $f$ between the optical field and the analytes while varying the size of pillars. The overlap integral is defined as:[21]

$$f = \frac{\int_{V_{low\ index}} \varepsilon \left|\vec{E}\right| dr^3}{\int_{V_{low\ index+dielectric}} \varepsilon \left|\vec{E}\right| dr^3} \quad (1)$$

Here, the volume integral in the numerator is the electric field energy outside of the Si pillars. The plot of the $f$ in relation to the Si duty cycle and width of pillars is shown in Fig. 3 (a). The Si duty cycle is defined as the length of Si pillars ($L$) divided by period. The $f$ increases as the decrease of Si duty cycle and the width of pillars, meaning the light confinement in the core is decreased and thus the sensitivity is enhanced. However, the optical loss will increase significantly. The photonic modes approach the light line of the cladding materials and are subject to more radiation loss resulting in quasi-guided modes [22]. We choose the Si duty cycle of 0.7 and a pillar size $L\times W\times H$ = 140 nm×600nm ×220nm considering the tradeoff between sensitivity and optical loss. The overlap 39.7% of TM modes is larger than 30.2% of TE modes with the same size pillar. Thus, a higher sensitivity for TM mode SWGRTRs is anticipated compared to the TE mode SWGRTRs with the same geometry. We analyze the coupling efficiency between the coupling length ($L_c$) and the gap ($G$) of the racetrack waveguide and subwavelength bus waveguide to minimize the influence of light in the racetrack [23]. We simulate the coupling efficiency shown in Fig. 3(b) changing with $L_c$ and $G$ by RSoft BeamPROP software. As shown in Fig. 3(b), larger coupling length is needed when the gap increases to achieve a maximum coupling strength from bus SWG waveguide to the racetrack waveguide; because the coupling strength is weakened as the gap is increased. The maximum coupling efficiency can be satisfied when gap is 140nm and the coupling length is approximately equal to 6μm by simulations [24, 25]. Specially, the racetrack resonator is a ring resonator when the $L_c$ equals 0. However, the footprint of racetrack resonator is less than that of circular ring with the same circumference.

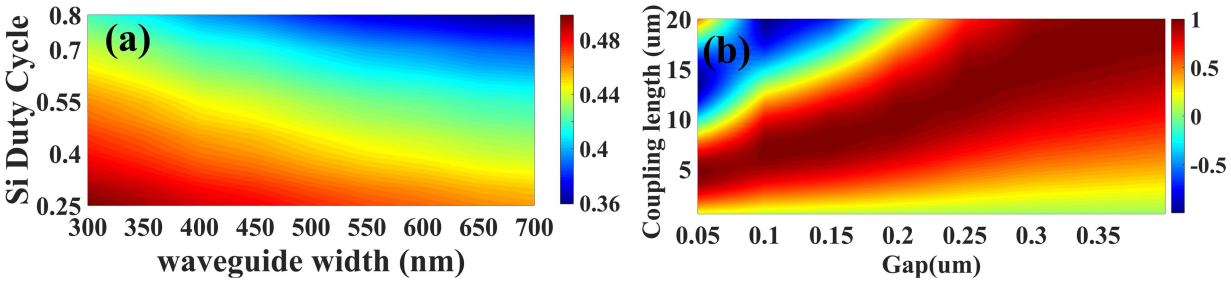


Fig. 3. (a) The plot of the overlap of light and matter changing with duty cycle and width of Si pillars. (b) The plot of the coupling efficiency changing with the coupling length $L_c$ and the gap $G$ around 1550 nm.

## DEVICE FABRICATION AND ANALYSIS

The devices with different coupling length $L_c$ (5.5μm, 6μm, 6.5μm, 7μm, and 7.5μm) are fabricated on SOI with a 220nm thick top silicon layer and a 3 μm thick buried oxide layer. The SWGRTR structures are firstly patterned with a single E-beam lithography process in the nanofabrication center at the University of Texas at Austin. The proximity effect is compensated in the design. Then, the patterns are transferred to the silicon dioxide (SiO2) hard mask, and to the silicon layer to form the silicon pillar layer through the reactive-ion-etching. Fig. 4(a) is the optical microscope image of the fabricated SWGRTR with coupling length $L_c$ of 6.5μm, in which light is coupled into the strip waveguide by the TM grating coupler, then coupled into SWG waveguide by the taper, and coupled out by the other taper and grating coupler. Fig. 4(b) is the scanning electron microscopy (SEM) image of the fabricated SWGRTR labeled in blue dash rectangular in Fig. 4(a). Figs. 4(c), 4(d) and 4(e) are the TM mode grating coupler, the magnified SEM images of the left taper between strip waveguide and SWG waveguide, and the coupling region of the bus SWG waveguide and SWG racetrack waveguide, respectively.

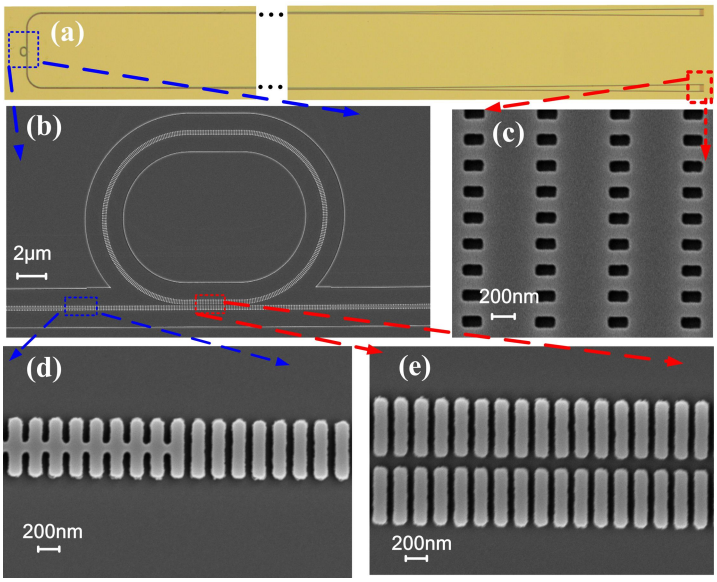


Fig. 4. (a) Optical microscope image of the fabricated SWGRTR with coupling length $L_c$ of 6.5μm. (b) Scanning electron microscopy (SEM) images of fabricated SWGRTR in blue dash box in (a). (c) The TM mode grating coupler in (a). The magnified SEM images of (d) the left taper between strip waveguide and SWG waveguide in blue dash box, and (e) the coupling region between the SWG bus waveguide and racetrack waveguide in red box region.

## DEVICE TESTS AND RESULTS

The fabricated devices are tested using a 1550 nm superluminescent LED (SLED) source and an optical spectrum analyzer (OSA). Light from the broadband SLED is guided through one terminal of the fiber array to the TM grating coupler on the chip and excites TM mode in the waveguide. Output light is detected by another terminal of fiber array, and optical spectrum is captured by the portable OSA.

To analysis the refractive index sensitivity of the fabricated SWGRTR, different concentrations of glycerol are applied and injected onto the chip surface through microfluidic channels. The testing transmission spectrum with 5 different $L_c$ (5.5μm, 6μm, 6.5μm, 7μm, and 7.5μm) in DI water is shown in Fig. 5(a). Fig. 5(b) shows a magnified view of the resonances in the red dashed rectangular in Fig. 5(a) with each resonance shifted for a relative distance to clarity. As seen in Fig. 5(b), the quality factor and the extinction ratio of the fabricated SWGRTRs are maximized when the coupling length is 6.5μm. The full-width at half-maximum (FWHM) of the resonance at 1555.9 nm in DI water is about 0.16 nm, corresponding to a quality factor of ~9800, and the extinction ratio is about 24.6dB. The optimized coupling length is 6.5μm in fabrication which is slightly different from the simulation results (6 μm). The fabrication induced roughness is possibly the reason for the discrepancy between the simulation and the fabrication.

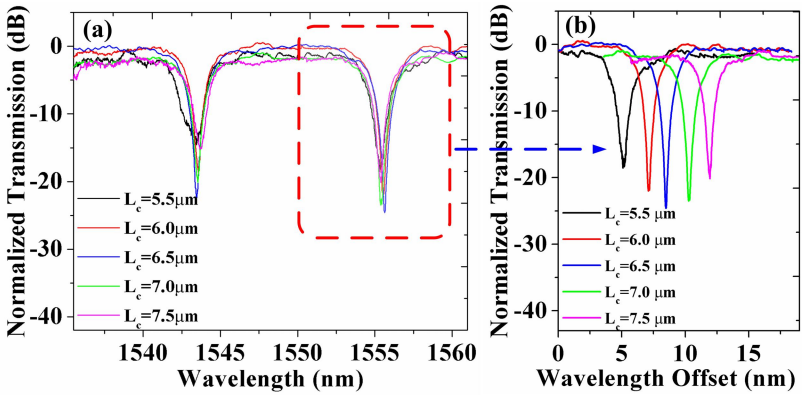


Fig. 5. (a) The testing transmission spectra of the fabricated 5 SWGRTRs with different $L_c$ (5.5μm, 6μm, 6.5μm, 7μm, and 7.5μm) in DI water. (b) Magnified resonance dips in red box region in (a), curves were shifted deliberately to show the difference.

The sensitivity of the SWGRTR is characterized by monitoring the resonance shift when different concentration solutions are consecutively injected onto the surface of the fabricated samples through microfluidic channels. The chip stage is kept at 25℃ with a temperature controller (Newport, Model 3040 Temperature Controller). The results for the SWGRTR with $L_c$ of 6.5μm are shown in Fig. 6(a). The space of narrow vertical dotted blue line represents the time when new concentration of glycerol solution is injected and the resonance shifts. Fig. 6(b) shows the stabilized transmission spectra after the new concentration solutions are applied. The refractive indices for 0%, 5%, 10%, and 20% concentration solutions of glycerol are 1.333, 1.340, 1.347 and 1.362, respectively [26]. Fig. 6(c) is the plot of linear fitting of the resonance shift in relation to the change of refractive index of the solution. The bulk sensitivity of the fabricated SWGRTR is about 429.7±0.4 nm/RIU.

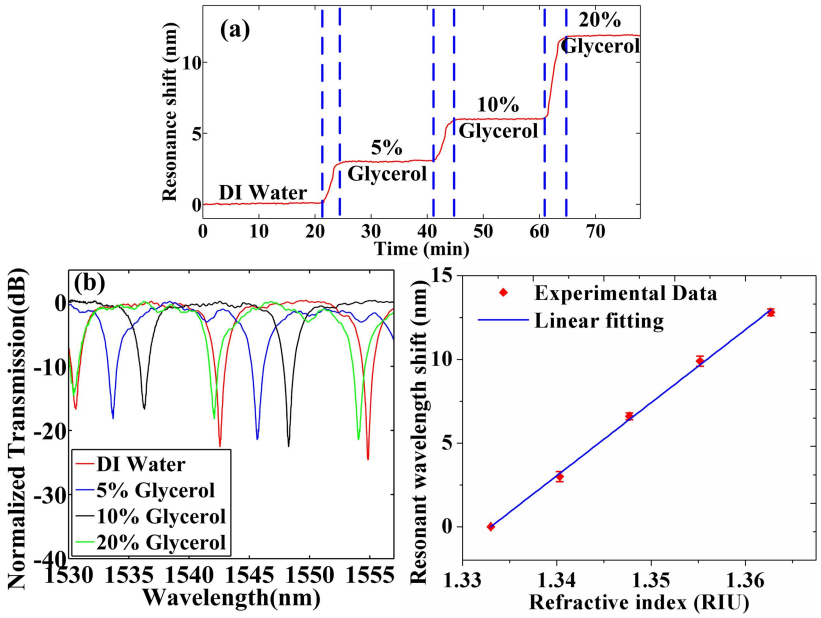


Fig. 6. (a) The results by monitoring the resonance shift for the fabricated SWGRTR with different concentration glycerol solutions. (b) The corresponding redshift of the transmission spectra for different concentration glycerol solutions (0%, 5%, 10% and 20%). (c) The linear fitting plot of the resonance shifts.

Then, to achieve the detection capability of the change of solution concentration, we analyze the *i*DL. The *i*DL is the minimum index change required to shift the resonance wavelength by one linewidth ($\Delta\lambda_{3dB}$), which is decided by both the sensitivity and the quality factor of resonator. However, for the racetrack resonator with the change of coupling length from 5.5μm to 7.5μm, the bulk sensitivity is almost the same, whereas the quality factor is a measure of the photon lifetime in the racetrack resonator, which relates to the total loss of resonator and will be changed significantly

with the coupling length. Therefore, we optimized the quality factor of racetrack resonator to achieve the lowest *i*DL at maximum *Q*. The *i*DL and quality factor of fabricated SWGRTRs with different $L_c$ are shown in Fig. 7 and fitted with Gaussian curve. It can be seen that the minimum *i*DL and maximum quality factor are achieved simultaneously when the coupling length equals 6.5 μm. At this coupling length, the minimum *i*DL of $3.71\times10^{-4}$ was achieved, which is 32.5% lower than the best value reported in SWG resonator sensor ($5.5\times10^{-4}$ RIU) [28]. The sensitivity of the SWGRTR is higher than that of TM mode strip waveguide ring resonators with waveguide thicknesses of 150 nm (247nm/RIU) and 220nm (238nm/RIU) [27]. The bulk sensitivity can be further improved by decreasing the Si duty cycle and the width of waveguide to increase the mode volume overlap.

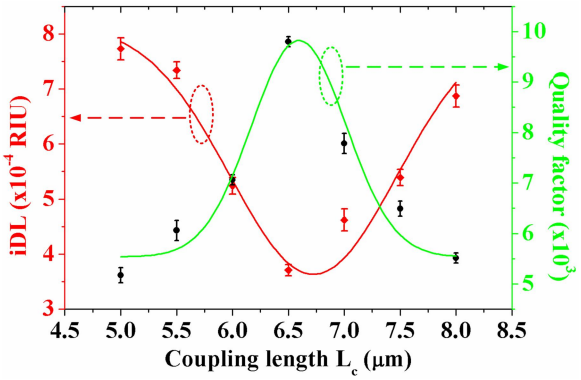


Fig. 7. The iDL and quality factor of the fabricated SWGRTRS with different $L_c$ in DI water.

## CONCLUSION

We have demonstrated a highly sensitive TM mode SWGRTR without deteriorating the high quality factor to enhance the intrinsic detection limit of sensor. Based on the simulation results, considering the tradeoff between light-analyte interaction and optical loss, we chose a pillar size of *L*=140 nm, *W*=600nm, and *H*=220nm. Simulation results show that the mode volume overlap of TM modes is 39.7%, which is larger than the 30.2% of TE modes with the same size of pillars. An optimal *Q* of 9800 in DI water has been observed when the coupling length, the gap, and silicon duty cycle are equal to 6.5 μm, 140nm, and 0.7, respectively, and the results of bulk index sensing test show a sensitivity of 429.7±0.4nm/RIU, which corresponds to a minimum *i*DL of $3.71\times10^{-4}$. The *i*DL is 32.5% lower than that of the circular ring resonator reported recently. In addition, the sensitivity can be further improved by using more aggressive mode volume overlap if better fabrication facility is available.

**Funding.** The research is supported by the Department of Energy Small Business Innovation Research (SBIR) program under the contract # DE SC-00113178. National Cancer Institute/National Institutes of Health (NCI/NIH) (Contract #: HHSN261201500039C).

**Acknowledgment.** Xiaochuan Xu and Ray T. Chen conceived the idea. L. Huang acknowledges the support by National Natural Science Foundation of China (No. 61372038), Fund of State Key Laboratory of Information Photonics and Optical Communications (Beijing University of Posts and Telecommunications)-IPOC2015ZC02, China and Postgraduate Innovation Fund of SICE, BUPT, 2015. L. Huang acknowledges the China Scholarship Council (CSC) (NO. 201506470010) for scholarship support.

## REFERENCES

1. X. Fan, I. M. White, "Optofluidic microsystems for chemical and biological analysis," Nat. photonics 5, 591 (2011).
2. W. C. Lai, S. Chakravarty, Y. Zou, R. T. Chen, "Multiplexed detection of xylene and trichloroethylene in water by photonic crystal absorption spectroscopy," Opt. Lett. 38, 3799 (2013).
3. S. Chakravarty, W. C. Lai, Y. Zou, H. A. Drabkin, R. M. Gemmill, G. R. Simon, S. H. Chin, R. T. Chen, "Multiplexed specific label-free detection of NCI-H358 lung cancer cell line lysates with silicon based photonic crystal microcavity biosensors," Biosens. Bioelectron. 43, 50 (2013).

4. H. Yan, Y. Zou, S. Chakravarty, C. J. Yang, Z. Wang, N. Tang, D. L. Fan, R. T. Chen, "Silicon on-chip bandpass filters for the multiplexing of high sensitivity photonic crystal microcavity biosensors", App. Phys. Let. 106, 121103 (2015).
5. Q. Quan, P. B. Deotare, and M. Loncar, "Photonic crystal nanobeam cavity strongly coupled to the feeding waveguide," Appl. Phys. Lett. 96, 203102-1 (2010).
6. B. Ahn, J. Kang, M. Kim, J. Song, B. Min, K. Kim, and Y. Lee, "One-dimensional parabolic-beam photonic crystal laser," Opt. Exp. 18, 5654 (2010).
7. K. Yao, Y. Shi, "High-Q width modulated photonic crystal stack mode-gap cavity and its application to refractive index sensing," Opt. Exp. 20, 27039 (2012).
8. L. Huang, J. Zhou, F. Sun, Z. F, H. Tian, "Optimization of One Dimensional Photonic Crystal Elliptical-Hole Low-Index Mode Nanobeam Cavities for On-chip Sensing," J. Lightwave Technol. 34, 3496, 2016.
9. X. Wang, X. Guan, Q. Huang, J. Zheng, Y. Shi, D. Dai, "Suspended ultra-small disk resonator on silicon for optical sensing," Opt. lett. 38, 5405 (2013).
10. S. M. Grist, S. A. Schmidt, J. Flueckiger, V. Donzella, W. Shi, S. T. Fard, J. T. Kirk, D. M. Ratner, K. C. Cheung, L. Chrostowski, "Silicon photonic micro-disk resonators for label-free biosensing," Opt. Exp. 21, 7994 (2013).
11. X. Fan, I. M. White, H. Zhu, J. D. Suter, and H. Oveys, "Overview of novel integrated optical ring resonator bio/chemical sensors," Lasers Appl. Sci. Eng. 64520M (2007).
12. T. Claes, J. G. Molera, K. De Vos, E. Schacht, R. Baets, and P. Bienstman, "Label-free biosensing with a slot-waveguide-based ring resonator in silicon on insulator," IEEE Photonics J. 1, 197 (2009).
13. V. Donzella, A. Sherwali, J. Flueckiger, S. M. Grist, S. T. Fard, L. Chrostowski, "Design and fabrication of SOI micro-ring resonators based on sub-wavelength grating waveguides," Opt. Exp. 23, 4791 (2015).
14. L. Huang, H. Tian, J. Zhou, Q. Liu, P. Zhang and Y. Ji, "Label-free optical sensor by designing a high-Q photonic crystal ring–slot structure," Opt. Commun. 335, 73 (2015).
15. L. Huang, H. Tian, J. Zhou and Y. Ji, "Design low crosstalk ring-slot array structure for label-free multiplexed sensing," Sensors 14, 15658, (2014).
16. C. A. Barrios, "Optical slot-waveguide based biochemical sensor," Sensors 9, 4751 (2009).
17. S. Chakravarty, A. Hosseini, X. Xu, L. Zhu, Y. Zou, R. T. Chen, "Analysis of ultra-high sensitivity configuration in chip-integrated photonic crystal microcavity bio-sensors," Appl. Phys. Lett. 104, 191109 (2014).
18. J. T. Kindt, M. S. Luchansky, A. J. Qavi, S. Lee, R. C. Bailey, "Subpicogram per milliliter detection of interleukins using silicon photonic microring resonators and an enzymatic signal enhancement strategy," Anal. Chem. 85, 10653 (2013).
19. X. C. Xu, H. Subbaraman, J. Covey, D. Kwong, A. Hosseini, and R. T. Chen, "Complementary metal–oxide–semiconductor compatible high efficiency subwavelength grating couplers for silicon integrated photonics," Appl. Phys. Lett.101, 031109 (2012).
20. Z. Wang, X. Xu, D. Fan, Y. Wang, H. Subbaraman, R. T. Chen, "Geometrical tuning art for entirely subwavelength grating waveguide based integrated photonics circuits," Scientific reports, 6 (2016).
21. N. Mortensen, S. Xiao, and J. Pedersen, "Liquid-infiltrated photonic crystals: enhanced light-matter interactions for lab-on-a-chip applications," Microfluid. Nanofluid. 4, 117 (2008).
22. L. C. Andreani, "Photonic bands and radiation losses in photonic crystal waveguides," phys. stat. sol.(b), 234, 139 (2002).
23. M. H. Lukas Chrostowski, Silicon Photonics Design, (academic, 2013).
24. J. C. Slater, Microwave electronics, (academic, 1950).
25. W. Bogaerts, P. D. Heyn, T. V. Vaerenbergh, K. D. Vos, S. K. Selvaraja, T. Claes, P. Dumon, P. Bienstman, D. V. Thourhout, R.Baets, "Silicon microring resonators," Laser Photonics Rev. 6, 47 (2012).
26. L. F. Hoyt, "New table of the refractive index of pure glycerol at 20 C," Industrial & Engineering Chemistry, 26, 329 (1934).
27. S. Schmidt, J. Flueckiger, W. Wu, S. M. Grist, S. T. Fard, V. Donzella, P. Khumwan, E. R. Thompson, Q. Wang, P. Kulik, X. Wang, A. Sherwali, J. Kirk, K. C. Cheung, L. Chrostowski, D. Ratner, "Improving the performance of silicon photonic rings, disks, and Bragg gratings for use in label-free biosensing," Proc. SPIE 9166, 91660M (2014).
28. J. Flueckiger, S. Schmidt, V. Donzella, A. Sherwali, D. M. Ratner, L. Chrostowski, K. C. Cheung, "Sub-wavelength grating for enhanced ring resonator biosensor," Opt. Exp. 24, 15672 (2016).